Manganese-Enhanced Magnetic Resonance Imaging Enables In Vivo Confirmation of Peri-Infarct Restoration Following Stem Cell Therapy in a Porcine Ischemia–Reperfusion Model

Rajesh Dash, MD, PhD; Paul J. Kim, MD; Yuka Matsuura, BS; Fumiaki Ikeno, MD; Scott Metzler, PhD; Ngan F. Huang, PhD; Jennifer K. Lyons, RVT; Patricia K. Nguyen, MD; Xiaohu Ge, MD, PhD; Cheryl Wong Po Foo, PhD; Michael V. McConnell, MD, MSEE; Joseph C. Wu, MD, PhD; Alan C. Yeung, MD; Phillip Harnish, PhD; Phillip C. Yang, MD

Background—The exact mechanism of stem cell therapy in augmenting the function of ischemic cardiomyopathy is unclear. In this study, we hypothesized that increased viability of the peri-infarct region (PIR) produces restorative benefits after stem cell engraftment. A novel multimodality imaging approach simultaneously assessed myocardial viability (manganese-enhanced magnetic resonance imaging [MEMRI]), myocardial scar (delayed gadolinium enhancement MRI), and transplanted stem cell engraftment (positron emission tomography reporter gene) in the injured porcine hearts.

Methods and Results—Twelve adult swine underwent ischemia–reperfusion injury. Digital subtraction of MEMRI-negative myocardium (intrainfarct region) from delayed gadolinium enhancement MRI–positive myocardium (PIR and intrainfarct region) clearly delineated the PIR in which the MEMRI-positive signal reflected PIR viability. Human amniotic mesenchymal stem cells (hAMSCs) represent a unique population of immunomodulatory mesodermal stem cells that restored the murine PIR. Immediately following hAMSC delivery, MEMRI demonstrated an increased PIR viability signal compared with control. Direct PIR viability remained higher in hAMSC-treated hearts for >6 weeks. Increased PIR viability correlated with improved regional contractility, left ventricular ejection fraction, infarct size, and hAMSC engraftment, as confirmed by immunocytochemistry. Increased MEMRI and positron emission tomography reporter gene signal in the intrainfarct region and the PIR correlated with sustained functional augmentation (global and regional) within the hAMSC group (mean change, left ventricular ejection fraction: hAMSC 85±60%, control 8±10%; *P*<0.05) and reduced chamber dilatation (left ventricular end-diastole volume increase: hAMSC 24±8%, control 110±30%; *P*<0.05).

Conclusions—The positron emission tomography reporter gene signal of hAMSC engraftment correlates with the improved MEMRI signal in the PIR. The increased MEMRI signal represents PIR viability and the restorative potential of the injured heart. This in vivo multimodality imaging platform represents a novel, real-time method of tracking PIR viability and stem cell engraftment while providing a mechanistic explanation of the therapeutic efficacy of cardiovascular stem cells. (***J Am Heart Assoc***. 2015;4:e002044 doi: 10.1161/JAHA.115.002044)

Key Words: ischemia–reperfusion injury • magnetic resonance imaging • manganese-enhanced magnetic resonance imaging • peri-infarct region imaging • stem cell imaging

Although revascularization attenuates myocardial injury after an ischemic event, patients often develop progressive heart failure.[1] Our clinical trials demonstrated that the presence of the peri-infarct region (PIR) is a major contributor to cardiovascular events and mortality in patients with ischemic cardiomyopathy.[2,3] Typically, the PIR is composed of a heterogeneous myocardium including live, injured, and dead tissue, resulting in electrical instability. Indeed, the degree of

heterogeneity in this vulnerable, yet salvageable, border zone has been shown to correlate with ventricular arrhythmias in patients.[2] Studies have demonstrated that the restoration of PIR viability and function improves electrical stability and outcomes in patients with ischemic cardiomyopathy.

Regenerative therapies have demonstrated the ability to target the PIR to improve ventricular function and remodeling in preclinical models of heart failure[4–6]; however, these studies have not demonstrated long-term engraftment of the transplanted stem cells or permanent restoration of the myocardium. Instead, it is believed that the transplanted stem cells undergo early lysis, which produces transient beneficial effects from the release of cytokines rather than cell engraftment.[7–11] To achieve sustained myocardial restoration, it may be necessary to achieve successful stem cell engraftment and increased PIR viability[7,11]; however, the absence of reliable in vivo tracking of these fundamental processes poses a major limitation to the translation of stem cell therapy.

In this study, we tested the hypothesis that our previously reported human amniotic mesenchymal stem cells (hAMSCs) from the placenta would enhance PIR viability.[12] The hAMSCs represent the epiblast of the inner cell mass of the embryo, giving rise to pluripotent extraembryonic mesodermal cells. These cells line the amniotic membrane at the fetal–maternal interface and demonstrate precardiac, immunomodulatory, and partially pluripotent properties.[12–14] Previous studies using mesenchymal stem cells showed significant improvement in cardiac ejection fraction and remodeling.[15] Consequently, we hypothesized that hAMSCs, which exhibit a favorable immunomodulatory profile for cardiac transplantation, would successfully restore cardiac function after ischemic injury. We used a unique in vivo myocardial viability imaging technology, manganese–enhanced magnetic resonance imaging (MEMRI), which allowed targeted imaging of viable cardiomyocytes through intracellular uptake of a manganese–based contrast agent by active L-type calcium channels without any prior genetic modification of the cells.[11] In our prior report, we demonstrated MEMRI's unique capability to characterize the injured myocardial tissue in a porcine ischemia–reperfusion model.[16] This differential uptake of manganese in the heterogeneous peri-infarct area denotes the injured, dead, and normal cardiomyocytes. This investigation exploits these unique properties of MEMRI to track the progressive changes in PIR viability in real time to understand the mechanism of stem cell therapy. Serial MEMRI characterized the changes in PIR viability, which exhibited an intermediate T1 signal relative to the remote region and intrainfarct region at baseline and an increased signal with cell therapy. The MEMRI signal increase correlated with the persistently positive positron emission tomography reporter gene (PET-RG) signal from the engrafted hAMSCs and subsequent restoration of regional and global function in the hAMSC-treated pigs.

Methods

Stem Cell Line Derivation

Human placentas were obtained from consenting healthy donors at Stanford University Medical Center (Stanford, CA). The protocol was approved by Stanford University's institutional review board and was described previously.[12] Briefly, the amniotic membrane was separated from the chorion, washed, enzymatically digested, and filtered. The cells were designated as amniotic mesodermal cells (hAMSCs).

Transduction of hAMSCs With Herpes Simplex Virus Thymidine Kinase PET-RG

The hAMSCs were transduced with a double-fusion PET-RG using an established protocol.[9] The PET-RG contained firefly luciferase for bioluminescence and herpes simplex virus thymidine kinase (HSV-tk) for PET. HSV-tk phosphorylates the radioisotope ^{18}F-FHBG to retain the isotope intracellularly to be detected as living cells expressing HSV-tk (Figure 1). The hAMSCs were incubated in lentivirus transduction medium (lentivirus multiplicity of infection of 10) for 24 hours and sorted by a fluorescence-activated cell sorter. Transduction was verified by green fluorescent protein fluorescence microscopy.
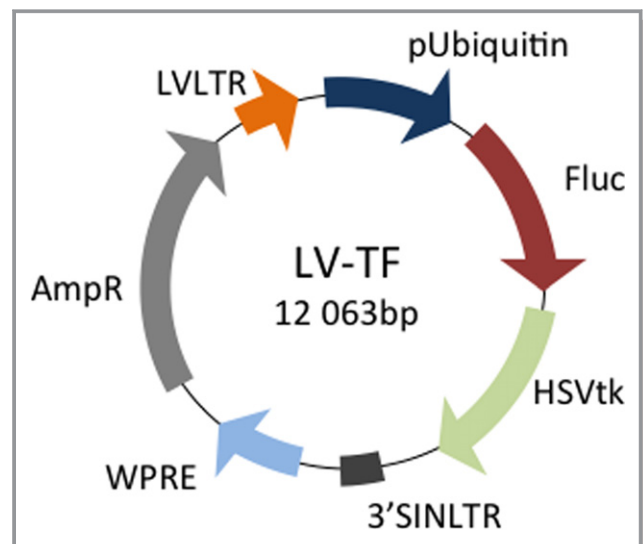

Figure 1. Lentiviral HSV-tk reporter gene construct. Viral vector map of HSV-tk positron emission tomography reporter gene construct used to transfect a subpopulation ($\approx$15 million of 80 million total) hAMSCs prior to cell transplantation. This construct contains dual reporter genes Fluc and HSVtk. HSVtk confers the ability to metabolize and retain the radioisotope ^{18}F-FHBG.[9] AmpR indicates ampicillin resistance; bp, base pairs; Fluc, firefly luciferase; hAMSCs, human amniotic mesenchymal stem cells; HSV-tk, herpes simplex virus thymidine kinase; LVLTR, lentiviral long terminal repeat; LV-TF, triple fusion lentiviral vector; SINLTR, self-inactivating long terminal repeat; WPRE, woodchuck hepatitis virus post-transcriptional response element.
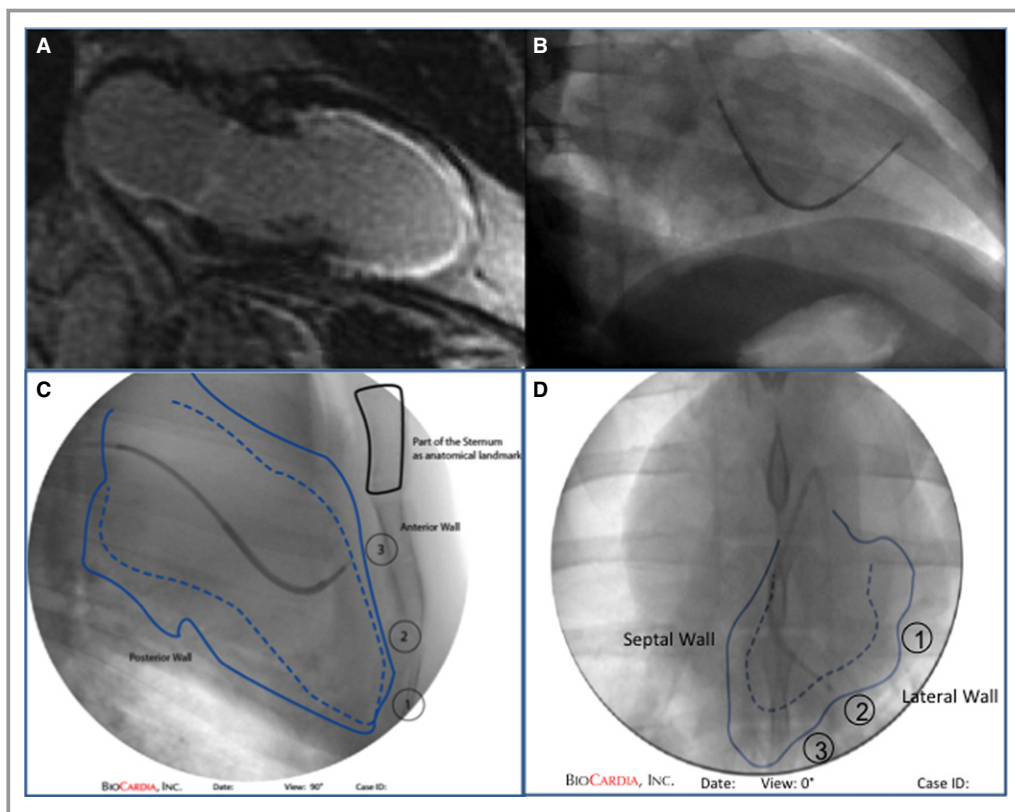
Figure 2. Fluoroscopically guided catheter cell delivery. Cell and control injections are targeted to the mid- to apical segments in each quadrant using (A) delayed gadolinium enhancement reference to the infarct zone and (B) biplane fluoroscopic mapping. Manual tracings documenting the locations of the injections are shown from (C and D) 2 different fluoroscopic projections. The sternum is used as an anatomical landmark, and the locations of injection are tracked numerically as marked.[19]

In Vivo MEMRI

For intravenous Mn^{2+} administration, EVP 1001-1 (Eagle Vision Pharmaceutical Corp) was used. This contrast agent contains nonchelated Mn^{2+} (12%) supplemented with 10% Ca^{2+}-gluconate. A dose of 0.7 mL/kg of EVP 1001-1 was used for systemic MEMRI in pigs, as described previously.[5]

Ischemia–Reperfusion Injury Procedure

Twelve Yorkshire swine (30 to 45 kg) were subjected to left anterior descending coronary ischemia–reperfusion injury for 60 minutes.[8,17] Swine were anesthetized (isoflurane 1% to 2%), and heparinized (300 IU/kg IV). An angioplasty balloon was inflated in the mid–left anterior descending artery for 60 minutes. To prevent arrhythmia, amiodarone 75 mg IV was administered before ischemia. In 1 pig, direct-current defibrillation (360 J) was performed successfully. There was no procedural mortality. After 60 minutes of ischemia, the balloon was deflated, and reperfusion was documented angiographically. The vessel sheath was removed, and the wound was closed. The animals were weaned from mechanical ventilation and recovered.

Porcine Myocardial Injection

Stem cells (or saline solution controls) were delivered intramyocardially to 8 infarct and peri-infarct zones using the Helix Helical Infusion System, a distal helical needle, and a Morph Universal Deflectable Guide Catheter (BioCardia Inc). Validated protocols for this fluoroscopically guided cell delivery system in large animals and humans have been described[18–21] (Figure 2). Briefly, the targeted region was defined by MEMRI and delayed gadolinium enhancement magnetic resonance imaging (DEMRI), and then right and left anterior-oblique ventriculograms were obtained. Each 0.5-mL cell injection contained $\approx 10 \times 10^6$ cells. Five control animals were injected with normal saline, and 7 animals were injected with hAMSCs.

One day prior to either cell delivery or saline injection (control), the swine were administered daily cyclosporine A (10 mg/kg oral administration, Sandimmune formulation; Novartis Pharma AG) for the experimental duration. At cell delivery, a 1-time dose of 15 mg/kg methylprednisolone sodium succinate (Upjohn) was administered intravenously.
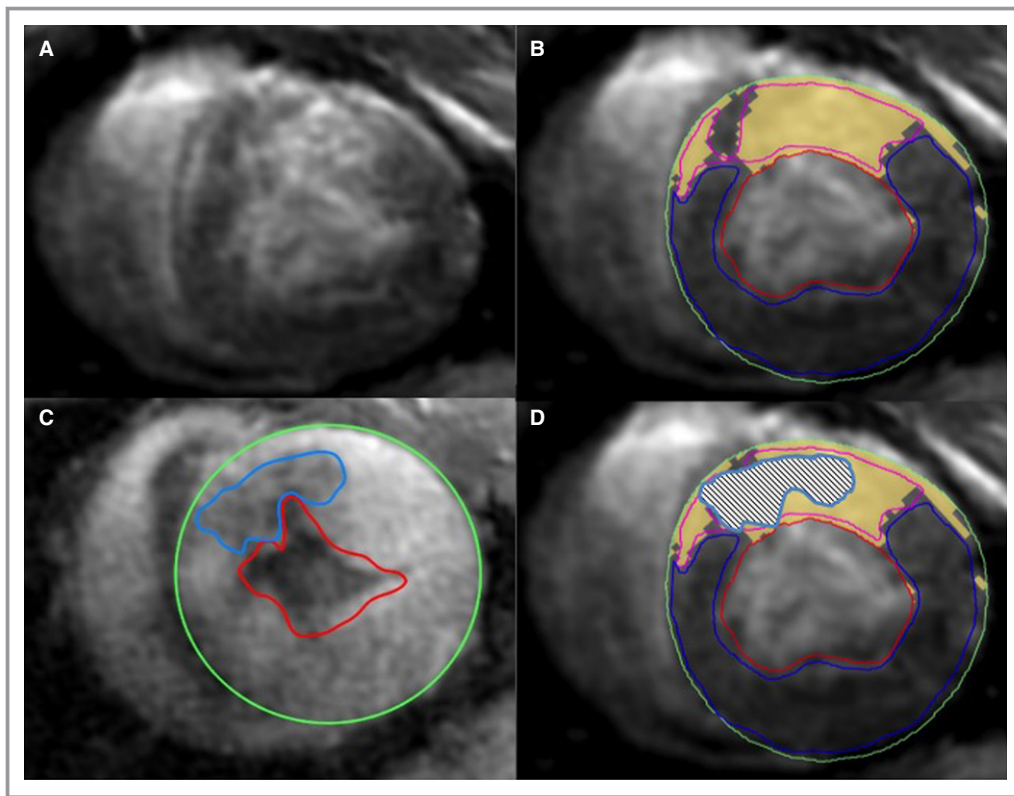
Figure 3. Regions of interest for DEMRI and MEMRI. Representative (A and B) short-axis DEMRI and (C) MEMRI images showing semiautomatic tracing of ROIs in a pig heart 6 weeks after human amniotic mesenchymal stem cell delivery. The signal threshold standard deviation method was used for DEMRI and MEMRI quantification with manual correction. Note the overall smaller MEMRI-defect area (blue ROI) compared with the yellow DEMRI-positive region. (D) Superimposed DEMRI and MEMRI infarct ROIs show the extent of PIR on either edge of the positive DEMRI regions still labeled yellow. DEMRI indicates delayed gadolinium enhancement magnetic resonance imaging; MEMRI, manganese-enhanced magnetic resonance imaging; PIR, peri-infarct region; ROI, region of interest.

Cardiac Magnetic Resonance Imaging Acquisition and Analysis

Cardiac magnetic resonance imaging (MRI) sequences for MEMRI and DEMRI were acquired and analyzed, as described previously.[5] Briefly, 3-T cardiac MRI was performed (Signa HDx 3.0T; General Electric) using an 8-channel chest coil and cardiac vector gating. The swine were anesthetized by isoflurane (1% to 2%). Following localizer images, steady-state acquisition was used (steady-state free procession: repetition time 3.8 ms; echo time minute full; flip angle 45°; slice thickness 10 mm; matrix 224 × 224; field of view 35) to obtain standard long- and short-axis cine images. MEMRI (fast gradient echo inversion recovery: repetition time 4.7 ms, echo time 1.3 ms, inversion time 400 ms, flip angle 15°, slice thickness 10 mm, matrix 224 × 192) was obtained 25 to 40 minutes after an EVP 1001-1 bolus 0.7 mL/kg IV. After MEMRI, a 30-minute washout preceded infusion of gadolinium for DEMRI. DEMRI (2-dimensional fast gradient echo inversion recovery: repetition time 4.6, echo time minute, flip angle 15°,

slice thickness 10 mm, matrix 256 × 256, field of view 35) was acquired 10 to 20 minutes after injection of gadolinium 0.2 mmol/kg (Magnevist; Bayer).

Images were analyzed using cmr[42] software (Circle Cardiovascular Imaging Inc) with semiautomatic left ventricular (LV) mass and volume tracing. MEMRI-defect and DEMRI-enhanced areas were designated as infarct areas. MEMRI-defect regions of interest (intrainfarct region, IIR) were traced semiautomatically using a −3 SD threshold method to designate signal defect regions, with manual correction (Figure 3). A digital subtraction of the MEMRI-defect region (IIR) from the DEMRI-positive region (PIR + IIR) yielded the PIR volume. The MEMRI images were analyzed for contrast/noise ratio variation between hAMSC and control hearts using the following equation: CNR=(SI of myocardial zone−SI of adjacent skeletal muscle)/SD of air. In this equation, CNR indicates contrast/noise ratio, SI indicates average signal intensity, and SD is the standard deviation.
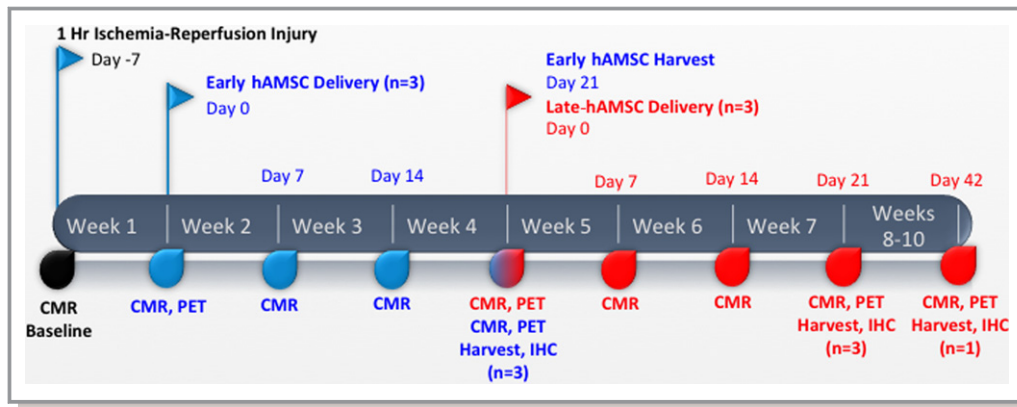
Figure 4. Timeline of cell-delivery experiments. Timeline outlining the ischemia–reperfusion injury and subsequent cardiac injections of hAMSC at both early (1 week, blue) and late (4 week, red) time points, in addition to the CMR, PET, harvest, and IHC performed for each group. CMR indicates cardiac magnetic resonance imaging; hAMSC, human amniotic mesenchymal stem cell; IHC, immunohistochemistry; PET, positron emission tomography.

Cardiac Positron Emission Tomography–Computed Tomography Acquisition

In 2 animals, 2 of 8 injection sites contained hAMSCs transduced with the HSV-tk PET-RG. Immediately following cell delivery and cardiac MRI, 40 mCi of ^{18}F-FHBG radioisotope were injected intravenously. After a 60-minute incubation (mean 536.5 MBq; range 370 to 777 MBq), positron emission tomography (PET) and computed tomography (CT) scans (Discovery LightSpeed Plus; GE Medical Systems) were performed in supine position, as described previously.[9] After an initial scout view (30 mAs, 120 kV), a nonenhanced 4-detector cardiac CT scan was obtained (section thickness 5 mm, table feed 38 mm/rotation, 0.8-second gantry rotation time, x-ray tube voltage 120 kV, tube current 150 mA). A 30-minute static PET scan was acquired. Transverse section reconstructions of the CT data set included section thicknesses of 5 mm with 4.25 mm spacing. PET images were reconstructed with an iterative algorithm (ordered-subset expectation maximization, 2 iterative steps, 28 subsets), with CT-based attenuation correction. The observed cardiac PET signal, normalized to ^{18}F-FHBG dosing and body weight, did not change significantly from day 0 to 3 weeks and 6 weeks after cell injection. No cardiac gating or respiratory motion correction was performed. A timeline of the experimental design is provided in Figure 4.

Immunohistochemistry

Deparaffinization/rehydration procedure

At room temperature, fixed, mounted sections were taken from the PIRs that were injected with hAMSCs and positive by MEMRI/PET imaging and from uninjected regions and were incubated in xylene. The sections were washed (2× each in 100% ethanol, 95% ethanol) and rinsed in distilled H$_2$0.

Antigen unmasking

Slides were incubated in 10 mmol/L sodium citrate buffer (pH 6.0) and brought to boil using a microwave, then maintained at 95°C to 99°C for 7.5 minutes. Slides were cooled and rinsed (3 times in distilled H$_2$0 and PBS).

Immunostaining

Slides were outlined using a PAP pen (Sigma-Aldrich, Inc), fixed in 4% paraformaldehyde for 20 minutes, and then rinsed (in distilled H20). The tissue was permeabilized with 0.1% Triton-X 100 (Sigma-Aldrich, Inc) for 30 minutes and washed in PBS for 5 minutes. The tissue was blocked using goat serum (Millipore, Inc) in 0.1% Triton-X 100 for 1 hour before washing 3 times in PBS (5 minutes). The slides were incubated with the primary anti-human nuclear antigen IgM monoclonal antibody BT69-7012-57 (Biotrend, Inc) at a 1:30 concentration, primary anti-human mitochondrial antibody (1:50), primary anti-human cardiac troponin T antibody (1:50), and primary anti-human alpha actinin antibody (1:50; Millipore, Inc). After washing for 5 minutes 3 times in PBS, secondary antibody was applied (rabbit anti-mouse IgM antibody [fluorescein isothiocyanate] or goat anti-mouse Alexa Fluor 488 at 1:200 in 2% goat serum for 1 hour). A signal amplification kit (Invitrogen, Inc) was used. The slides were then washed 3 times in PBS (5 minutes) and mounted (Vector Labs, Inc) with coverslips. Fluorescent microscopy was used for human nuclear antigen cell visualization.

Data Analysis and Statistics

Coregistration of MRI and PET imaging was performed using AZE Technologies analysis software. Student *t* test and ANOVA were used for group comparisons of contrast/noise ratio. All numerical results listed in text and figures included mean±SD. Linear regression and Spearman nonparametric correlation analysis was performed for MEMRI contrast/noise ratio and PET signal comparison.

Results

hAMSC Harvest and HSV-tk PET-RG Transduction

From each human placental harvest, $\approx 80 \times 10^6$ hAMSCs were generated at 1 to 2 cell passages (Figure 5A). To enable in vitro and in vivo colocalization, a subset of hAMSCs (20%) was transduced with a luciferase/HSV-tk PET-RG.[22] The in vitro bioluminescence signal remained strong for 6 weeks after transduction, with no reduction (Figure 5B). These transduced hAMSCs were used to verify cell injection sites and long-term engraftment in vivo. The hAMSCs express a unique cell surface marker profile, which includes the following subsets: (1) pluripotent: SSEA-3 (6.2±2%), SSEA-4 (20.4±5%), and TRA-1 to 81 (2±1.2%); (2) mesodermal: Thy1 (16.5±3%); (3) precardiac progenitor: c-kit (9.8±1.1%); (4) immunomodulatory: HLA-G (8.3±2%, apoptosis of activated $CD8^+$ and inhibition of $CD4^+$ T cells), HLA-E (7.3±5%, inhibition of natural killer and cytotoxic T-lymphocytes cells), intercellular adhesion molecule (25.1±4%), CD59 (98±1.2%, prevention of complement-mediated cell lysis), and absence of HLA-DR (0.4±0.1%). Flow cytometry of HLA-DR, CD59, HLA-G, and c-kit and immunostain of Thy-1, SSEA-4, and c-kit are shown in Figure 6A through 6E.

hAMSC Delivery Produces Sustained Improvements in LV Function and Remodeling

Serial cardiac MRI analyses demonstrated that hAMSCs conferred significant and sustained improvements in systolic function in the early hAMSC (acute injury) group (85±34% increase in LV ejection fraction [LVEF] from preinjection level, n=4, *P*<0.05) measured on days 7 and 21 after injection (Figure 7A and 7B, Videos S1 and S2). Conversely, the control animals, which received either normal saline (n=4) or lysed hAMSCs (n=1), exhibited no improvement in LVEF over the same 21-day period. In the late-hAMSC (chronic injury) group, functional restoration of a similar magnitude and time course to the early hAMSC group was observed (56±18% increase from preinjection LVEF, n=3, *P*<0.05) (Figure 7A) and remained stable long term. The hAMSC-treated animals exhibited an absolute LVEF increase of 14±6% (*P*<0.05) on
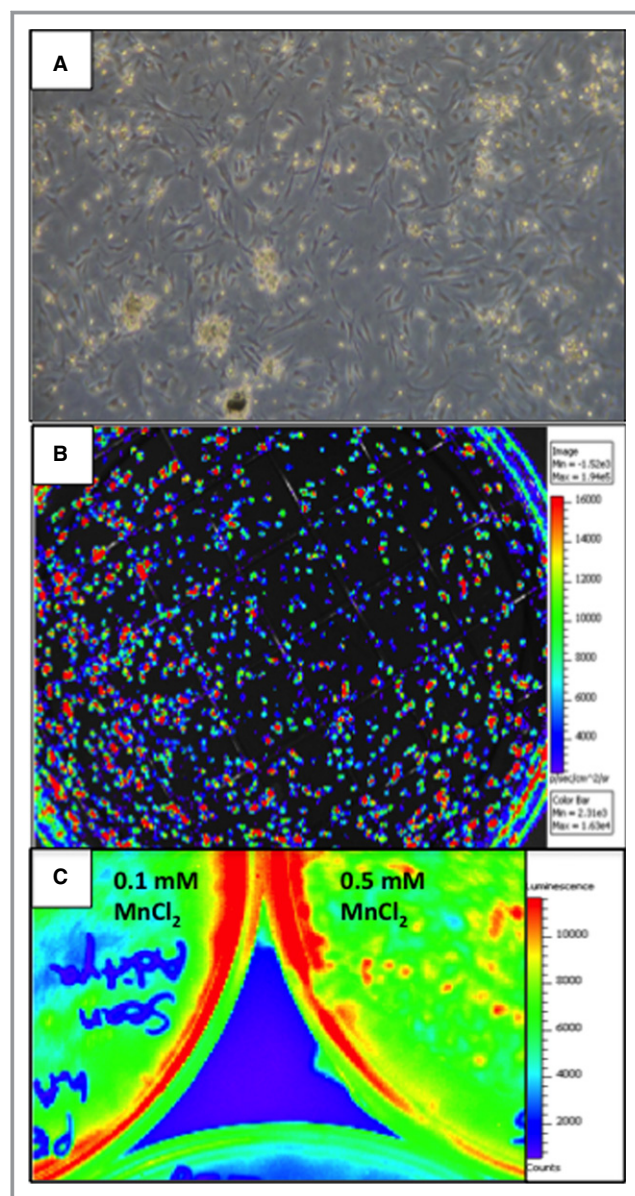
Figure 5. Isolation, culture, and reporter gene transduction of hAMSCs. A, A subset of hAMSCs was cultured for 6 weeks after transduction with the herpes simplex virus thymidine kinase positron emission tomography reporter gene and showed expansion properties similar to nontransduced hAMSCs. B, Robust in vitro BLI signal from hAMSCs 6 weeks after transduction with the HSV-tk and firefly luciferase double-fusion reporter gene. C, BLI of plated hAMSCs 5 days after Mn^{2+} labeling. Note the preserved BLI signal at 0.1 and 0.5 mmol/L $MnCl_2$, indicating no impairment of cell survival with Mn^{2+} labeling. BLI indicates bioluminescence; hAMSCs, human amniotic mesenchymal stem cells.

day 21 after injection versus a control group ejection fraction change of −2±5%. One late-hAMSC animal was monitored for an additional 3 weeks (total 6 weeks after hAMSC treatment) and maintained improved LVEF, suggesting durable augmentation of cardiac function.
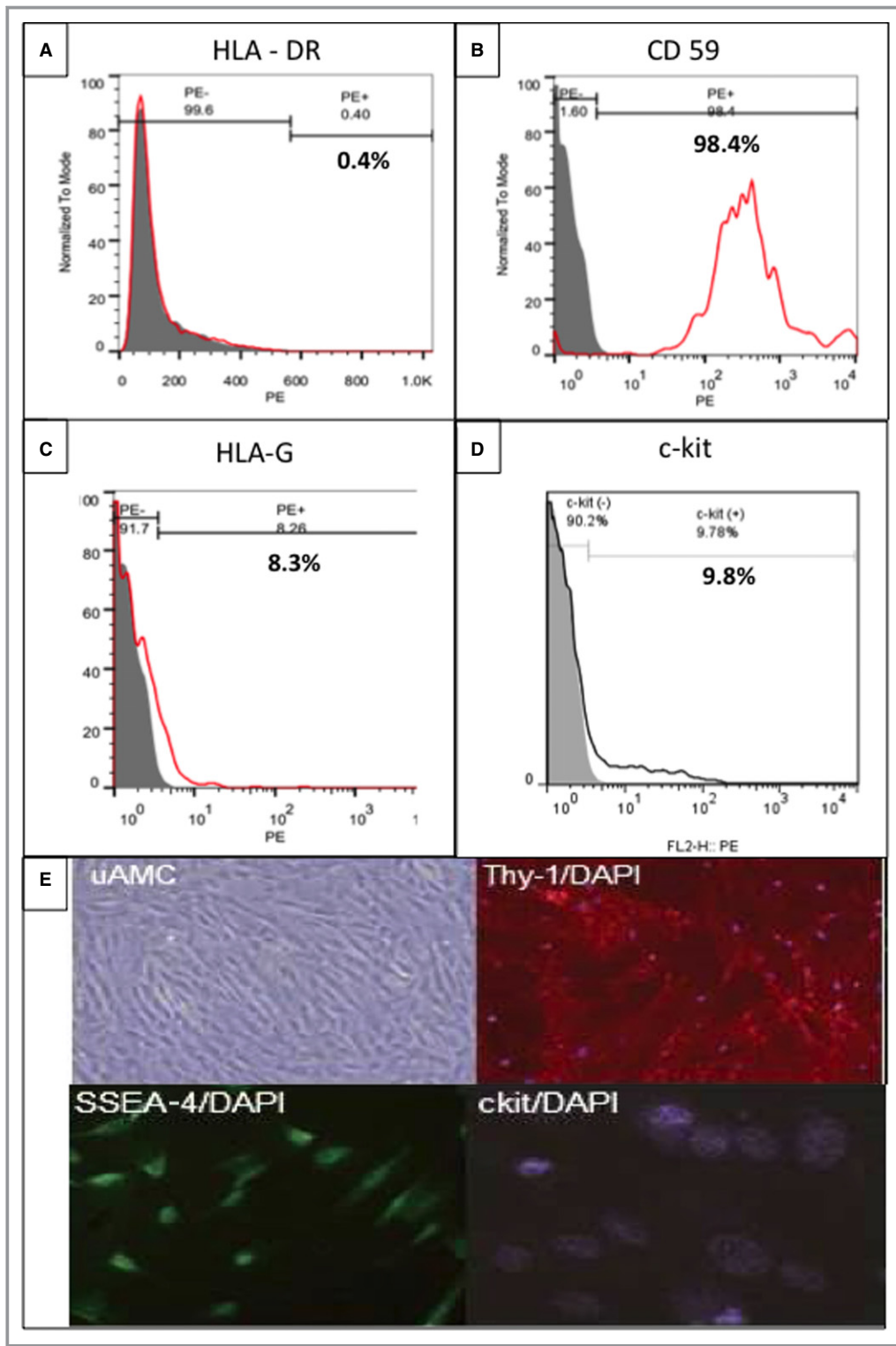
Figure 6. Flow cytometry and immunohistological characterization of hAMSCs. A, Flow cytometry analysis indicated 0% HLA-DR–positive hAMSCs. PE, phycoeryhthrin. B, Flow cytometry analyses showed a high proportion of CD59 positive cells, with smaller proportions of (C) HLA-G; (D) c-kit–positive hAMSCs; and (E) immunohistological evidence of hAMSC cell surface markers, including uAMC, Thy-1, SSEA-4, and c-kit. hAMSCs indicates human amniotic mesenchymal stem cells.
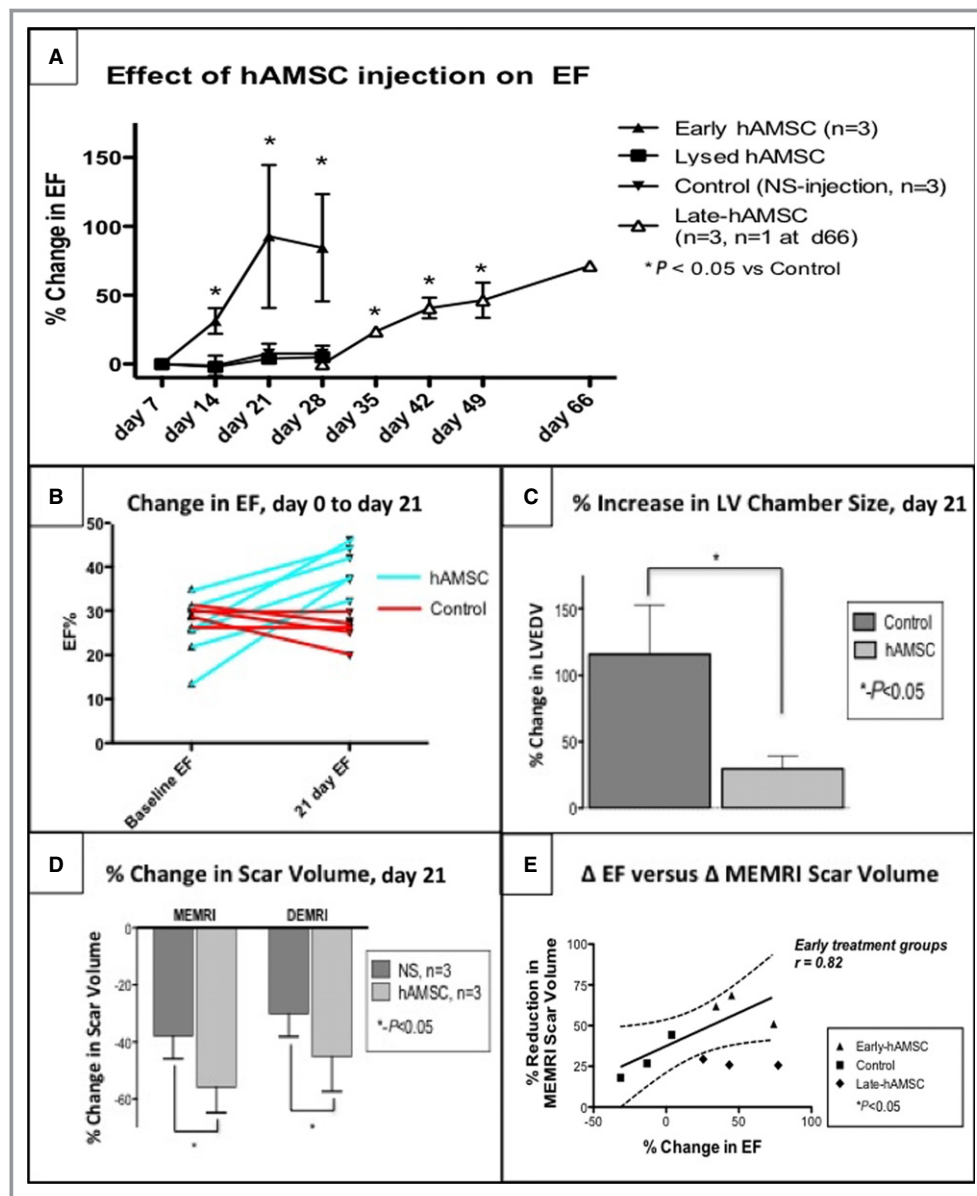
Figure 7. LVEF and remodeling improvements in the hAMSC-treated hearts. hAMSC treatment led to sustained improvement in cardiac function. A, Mean percentage of LVEF increases in early and late-hAMSC hearts vs control hearts compared with post-IR, preinjection LVEF. The hAMSC-treated swine (light green) exhibited a significant LVEF increase immediately after hAMSC delivery (day 7) that was sustained for 21 days after delivery (day 28 after IR, day 21 after injection). NS-injected and lysed hAMSC controls showed no improvement in LVEF over the same time period. Late-hAMSC hearts, which received hAMSCs 28 days after IR injury, exhibited a predictable, significant, and steady rise in LVEF after cell delivery. B, Absolute LVEF changes before and after injection showed a consistent increase in the LVEF in hAMSC-treated swine and a consistent decrease in LVEF in the control group. C, LVEDV in hAMSC hearts exhibited 86% less chamber dilatation (percentage change in LVEDV) than the control group, indicating improved LV remodeling due to hAMSC delivery. D, MEMRI/DEMRI infarct size improvement in hAMSC-treated hearts, which exhibit a significantly lower MEMRI-defect volume and positive DEMRI scar volume compared with control hearts at 21 days after hAMSC therapy. E, A strong linear correlation was observed between the percentage change in LVEF and the percentage of infarct size reduction by MEMRI scar volume in the early hAMSC IR hearts (values expressed as percentage of total LV myocardium). Notably, the degree of scar reduction in late-hAMSC hearts is not as pronounced as in the early hAMSC hearts, despite similar LVEF increases. DEMRI indicates delayed gadolinium enhancement MRI; EF, ejection fraction; hAMSC, human amniotic mesenchymal stem cell; IR, ischemia-reperfusion; LV, left ventricular; LVEDV, left ventricular end-diastolic volume; MEMRI, manganese-enhanced magnetic resonance imaging; NS, normal saline.

A pathologic feature after myocardial infarction is severe LV dilatation. The hAMSC-treated hearts exhibited preserved LV end-diastolic volume, increasing only 30±10% (P<0.05) in the early hAMSC group compared with baseline, whereas the control group LV end-diastolic volume increased 116±37% (P<0.05) (Figure 7C). LV mass was not changed (hAMSC +18±16 g, normal saline +9±22 g; P>0.05). In the late-hAMSC group, LV dilatation was also attenuated (LV end-diastolic volume increase +71±25%, P<0.05 versus control). In summary, early and late-hAMSC groups showed significant and sustained functional and remodeling benefits compared with the control group.

hAMSC Delivery Enhances Regional Myocardial Viability and Function

The measurement of regional scar and viability was used to assess myocardial preservation. Early hAMSC animals exhibited a greater reduction in infarct size (P<0.05), measured by the postdelivery changes in DEMRI enhancement and MEMRI defect, compared with the control animals (Figures 8A through 8E and 7D). Furthermore, in the early hAMSC group, the increased viability of the PIR measured by MEMRI correlated with improved LVEF (Figure 7E). To determine whether the hAMSCs augmented cardiac function locally or globally, the radial thickening percentage and the segmental PIR MEMRI signal from days 0 to 21 after injection were compared with the control group in the corresponding mid- to apical segments (Figure 9). Radial thickening worsened in the control group, whereas it significantly improved in the hAMSC group (Figure 9A and 9B). When plotted against the corresponding change in the segmental MEMRI signal/noise ratio, the hAMSC group exhibited improved MEMRI signal/noise ratio with improved thickening, whereas the control group exhibited a reverse pattern (Figure 9C). Consequently, MEMRI signal correlated with regional myocardial restoration in the hAMSC-treated segments.

Prolonged In Vivo Signal of the Viable Engrafted hAMSCs Using Serial PET-CT

Serial cardiac PET-CT scans on days 0, 7, 21, and 38 were performed using an ^{18}F-FHBG radioisotope that is phosphorylated only by live, transduced cells to generate a PET signal. At each time point, an apical–septal PET signal (≈25-fold higher than surrounding myocardium) was observed that colocalized with the sites of cell injections (Figure 10A). These hyperintense foci persisted throughout the duration of the study, and the specificity of the PET-RG signaling mechanism confirmed engraftment of the transplanted cells (Figure 10C and 10D).[9] When plotted according to the

American Heart Association 16-segment model, the PET signal intensities from each myocardial segment showed a significant linear correlation with PIR MEMRI signal intensity (P<0.05) (Figure 10E and 10F). These persistent in vivo PET-RG foci suggest that hAMSCs survived in vivo for at least 6 weeks after injection in this swine ischemia–reperfusion model. More important, the engraftment of these live reporter gene–transduced hAMSCs was tracked longitudinally and provided real-time correlation of cell therapy with functional restoration.

Histopathological Evidence of Prolonged In Vivo Survival of Transplanted hAMSCs

Immunostaining from these colocalized apical–septal segments stained positive for anti-human nuclear antigen and anti-human mitochondrial antibodies 6 weeks after hAMSC delivery, confirming the engraftment of hAMSCs and their PET-RG signal at a prolonged time point (Figure 11A through 11F). Moreover, these hAMSC clusters were negative for cardiac troponin or α-actinin staining, suggesting no differentiation to cardiac lineage (Figure 11G and 11H). These immunohistological findings validated in vivo PET-CT detection of stem cell engraftment in a large animal myocardial injury model and confirmed the mechanistic correlation between stem cell engraftment and functional restoration.

Discussion

This study introduced an in vivo MEMRI technology that monitors regional myocardial restoration while providing mechanistic insight of cell therapy longitudinally. Real-time monitoring of the regional myocardial viability by the engrafted hAMSCs in the injured porcine myocardium was confirmed by colocalized cardiac PET-CT and immunofluorescent signals. These findings demonstrated the widespread utility of MEMRI to track the therapeutic efficacy of stem cell therapy by confirming the ability to restore injured cardiomyocytes in the peri-infarct myocardium.[16]

A major obstacle to cardiovascular stem cell therapy is the inability to monitor the engraftment of the transplanted stem cells in vivo, which has been demonstrated to correlate with improved myocardial function.[7,10,23,24] A positive PET-RG signal from the engrafted stem cells was validated through histological colocalization with immunofluorescence for human antigens unique to the transplanted hAMSCs. The significantly increased MEMRI signal in PIR may indicate progressive enhancement of myocardial viability and functional capacity, suggesting salvage and/or regeneration of the injured myocardium by hAMSCs. The immunostain was negative for cardiac troponin or α-actinin stain within the
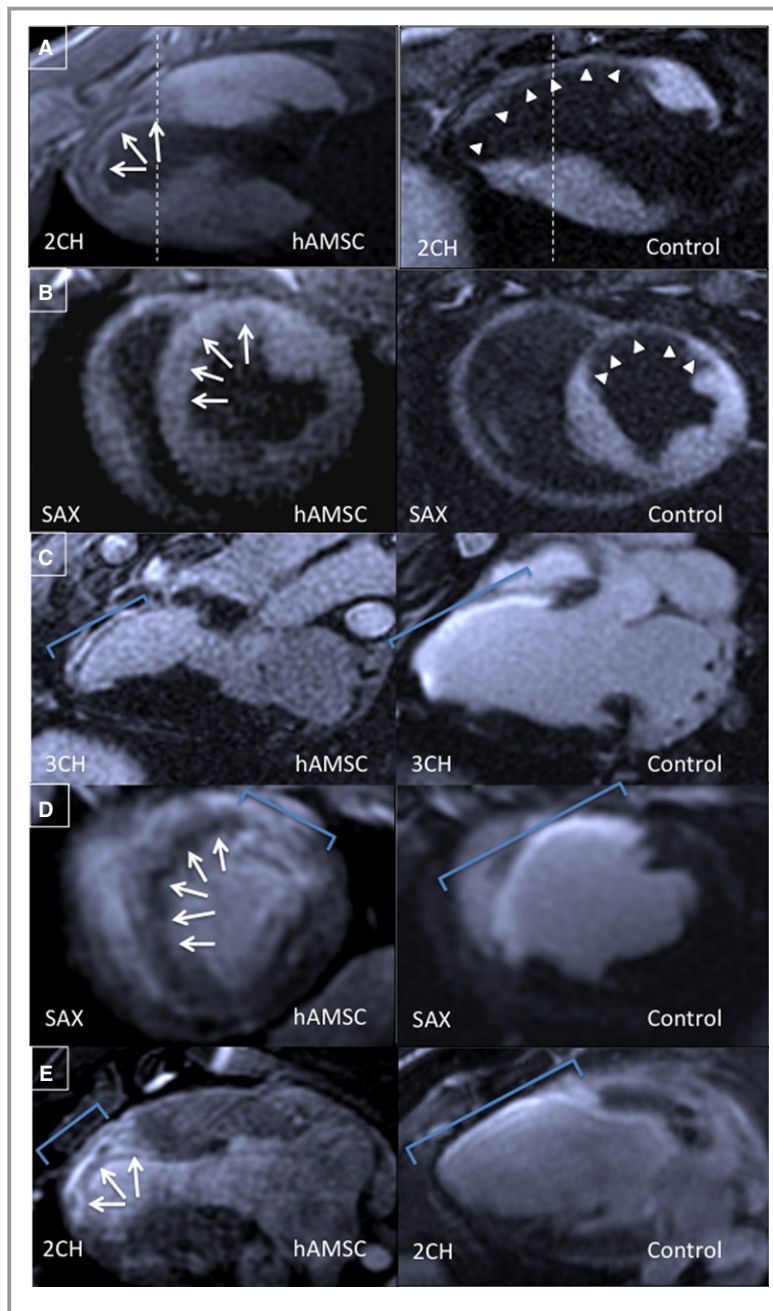
Figure 8. DEMRI and MEMRI for hAMSC- and control-injected hearts. Representative MEMRI images shown in (A) 2-chamber and (B) short-axis views from the same animals demonstrate positive MEMRI signals (white arrows) throughout the infarct zone in the hAMSC group, resulting in a reduced MEMRI-defect region and increased contrast/noise ratio compared with the control group MEMRI-defect area (white arrowheads). Corresponding DEMRI images from the hAMSC and control groups 21 days after injection in (C) 3-chamber, (D) short-axis, and (E) 2-chamber views. Smaller regions of positive delayed enhancement in the anteroseptal walls of the hAMSC group are noted. Blue brackets delineate the region of positive DEMRI. hAMSC-treated hearts also exhibit increased viability in the expected infarct zone, with viable myocardium mixed with scar in the DEMRI and MEMRI images (white arrows, D and E). The region of transmural DEMRI-positive myocardium is substantially reduced (C through E, blue brackets). 2CH indicates 2-chamber; 3CH, 3-chamber; DEMRI, delayed gadolinium enhancement magnetic resonance imaging; hAMSC, human amniotic mesenchymal stem cell; MEMRI, manganese-enhanced magnetic resonance imaging; SAX, short-axis.
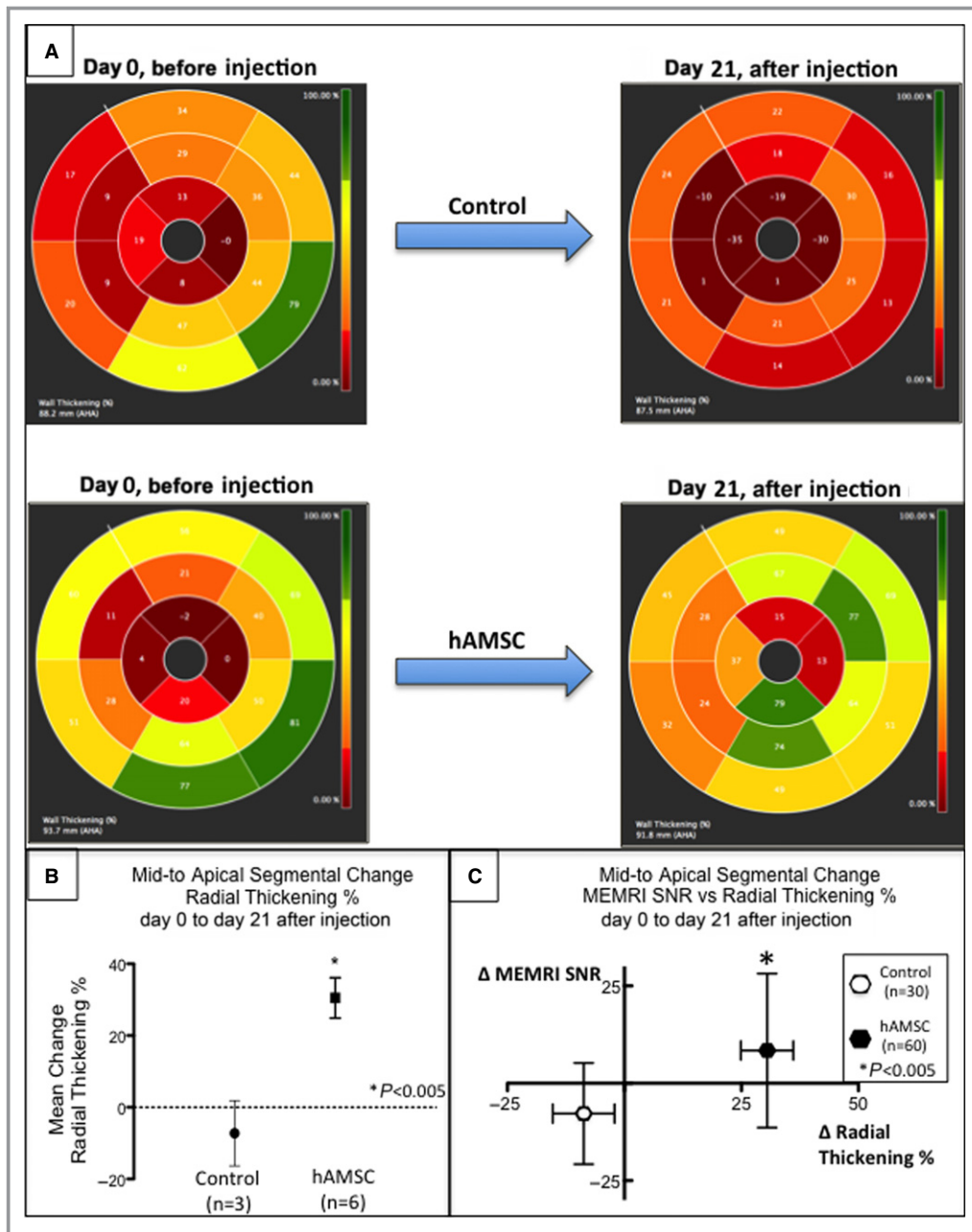
Figure 9. Segmental improvement in hAMSC-treated hearts by percentages of both MEMRI and radial thickening. A, Polar maps depicting representative percentages of radial thickening at days 0 to 21 after injection from the mid- to apical segments (segments 7 to 16 of American Heart Association 16-segment model) of the control and hAMSC-treated hearts. Note the significant improvement (brighter color map in mid- to apical segments) in the hAMSC-treated heart compared with control (darker color map in day 21 mid- to apical segments). B, Percentage of mid- to apical segmental radial strain measurements in control vs hAMSC-treated hearts. Note the significant increase in mean percentage of segmental radial strain in hAMSC hearts. C, Scatterplot of change in segmental MEMRI signal (*y*-axis) vs change in percentage of radial thickening (*x*-axis) from both control (open symbols) and hAMSC-treated (closed symbols) hearts. Note the distribution of hAMSC-treated hearts in the upper right quadrant, reflecting an association of improved MEMRI signal of myocardial viability and improved radial thickening. Conversely, the control hearts exhibited worsened MEMRI signal and lower percentage of radial thickening, consistent with the lack of functional recovery in the control hearts. hAMSC indicates human amniotic mesenchymal stem cell; MEMRI, manganese-enhanced magnetic resonance imaging; SNR, signal/noise ratio.
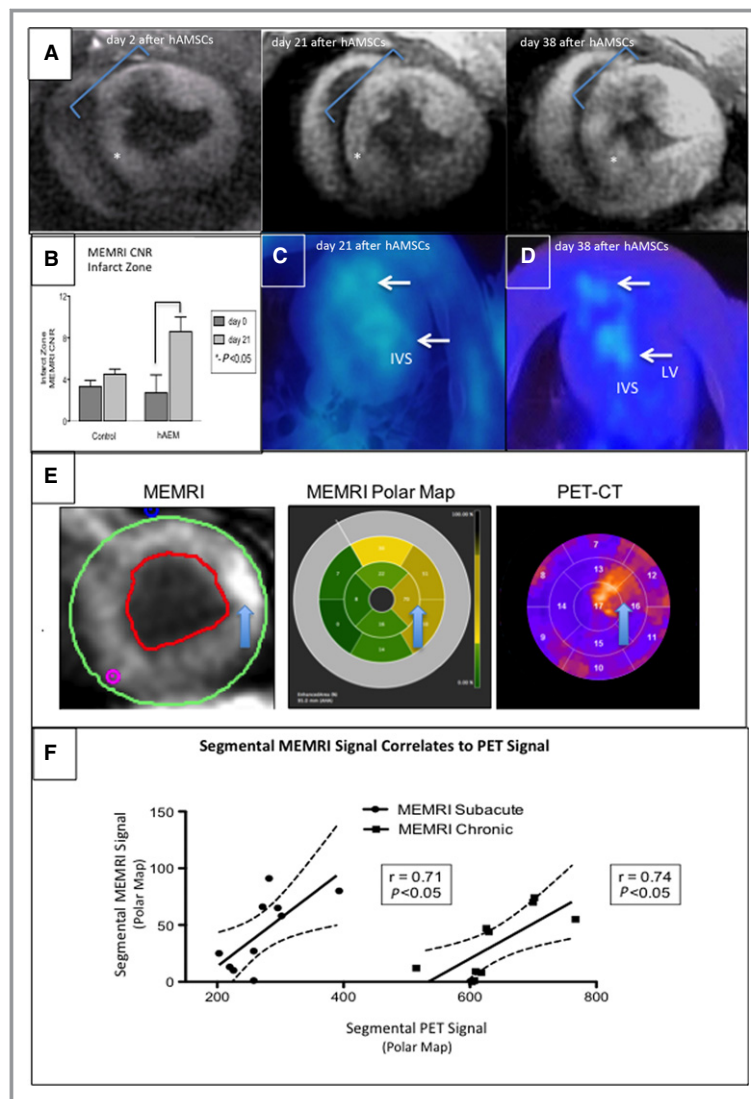
Figure 10. MEMRI and PET colocalization of the hAMSC-injected hearts. In vivo confirmation of MEMRI signal for live hAMSCs within the myocardium of a hAMSC-injected swine is shown. hAMSCs were delivered 1 week after ischemia–reperfusion injury into the peri-infarct zones of the mid- to apical infero- and anteroseptum. A, SAX MEMRI image on day 2 with a characteristic MEMRI defect in the infarct zone (blue region of interest). Note area of inferoseptum with increased signal (star). Serial MEMRI shows increasing signal intensity in inferoseptum on days 21 and 38 after cell delivery, with overall increased signal within the infarct zone. B, Absolute increase in MEMRI CNR of the infarct zone in the hAMSC-treated vs control (normal saline–injected) hearts on day 21 after hAMSC delivery. C and D, Axial PET reporter gene signals from hAMSC populations in the apical septum, confirming specific live hAMSC activity on days 21 and 38 (IVS, LV). E, SAX MEMRI images (left) from an early hAMSC animal with traced endo- and epicardial contours; corresponding polar maps (middle) of MEMRI signal from the mid- to apical slices of the LV (the regions of hAMSC injection), with yellow and tan colors indicating increasing signal intensity; polar maps (right) from corresponding PET images. Note the similar patterns between MEMRI and PET polar maps. Arrows denote the focal signal in both MEMRI and PET images. F, Significant linear correlation of MEMRI signals (y-axis, signal intensity units) and PET signals (x-axis, signal intensity units) for both early hAMSC (left plot) and late-hAMSC (right plot) hearts. CNR indicates contrast-to-noise ratio; CT, computed tomography; hAMSCs, human amniotic mesenchymal stem cells; IVS, interventricular septum; LV, left ventricle; MEMRI, manganese-enhanced magnetic resonance imaging; PET, positron emission tomography; SAX, short-axis.
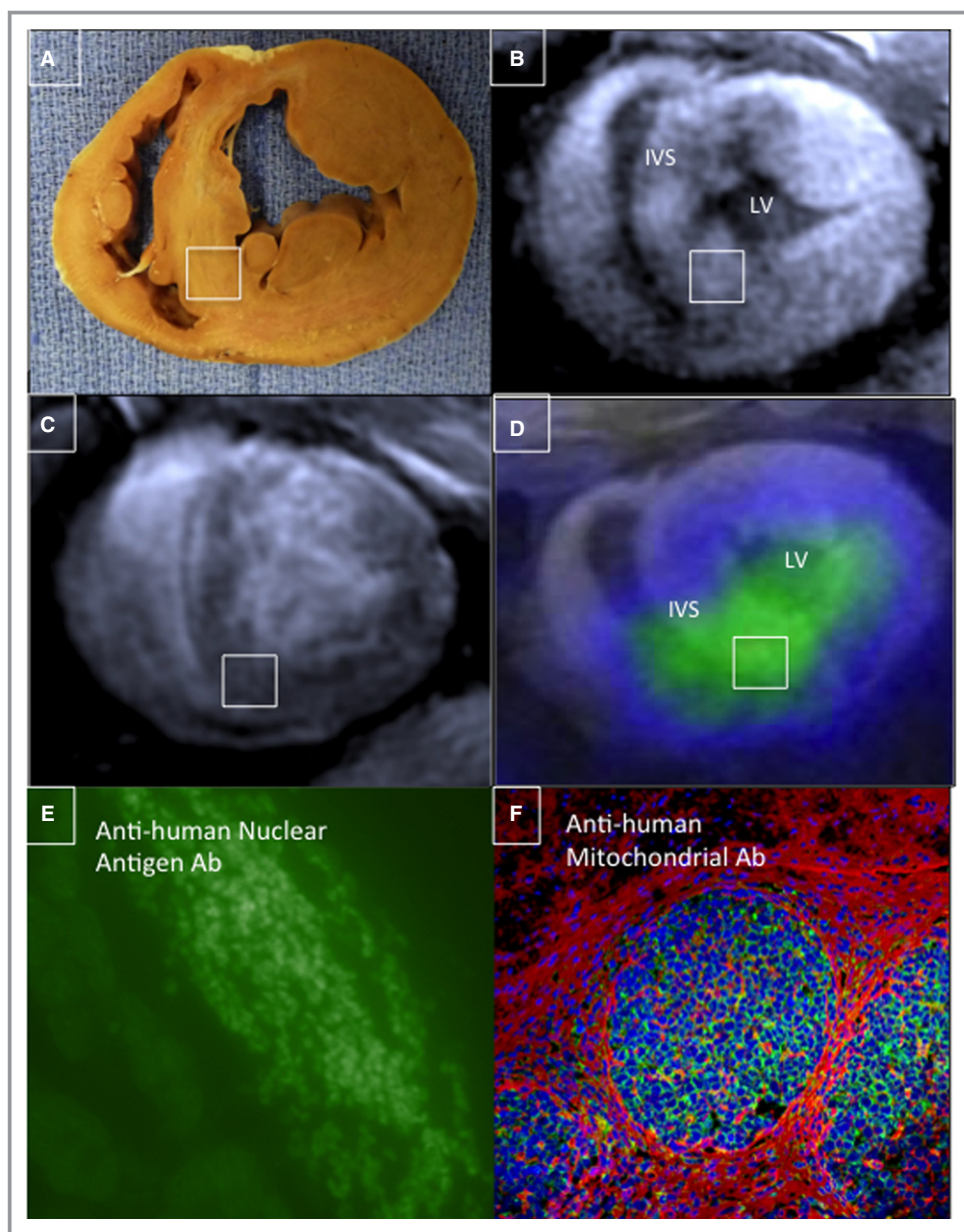
Figure 11. Immunostaining confirmed intact hAMSC populations in vivo. A, Gross SAX section of a hAMSC-injected heart (6 weeks after cell delivery) demonstrated prominent anterior and inferoseptal peri-infarct segments, which were hAMSC injection sites (note: inset white box corresponds to MEMRI, DEMRI, and PET images and to the immunostaining tissue specimen). B, A bright focus (white box) of MEMRI signal is detected within the inferoseptal peri-infarct region corresponding to cell injection site. C, Matched DEMRI SAX image shows preserved myocardium (null signal) throughout most of the septum. D, 3-dimensional coregistration of PET-RG and MEMRI images acquired on the same day, showing a colocalized focus of intense inferoseptal signal from the PET-RG–transduced hAMSCs and increased MEMRI signal (white box). E and F, Myocardial sections stain positive for (E) anti-human nuclear antigen Ab and (F) anti-human mitochondrial antigen Ab, confirming the presence of live hAMSC populations up to 6 weeks after cell transplantation in these matched MEMRI and PET-positive regions. G and H, These same cell clusters are negative for both anti-α-actinin and anti-troponin Ab staining. Ab indicates antibody; DEMRI, delayed gadolinium enhancement magnetic resonance imaging; hAMSC, human amniotic mesenchymal stem cell; IVS, interventricular septum; LV, left ventricle; MEMRI, manganese-enhanced magnetic resonance imaging; PET, positron emission tomography; PET-RG, positron emission tomography reporter gene; SAX, short-axis.
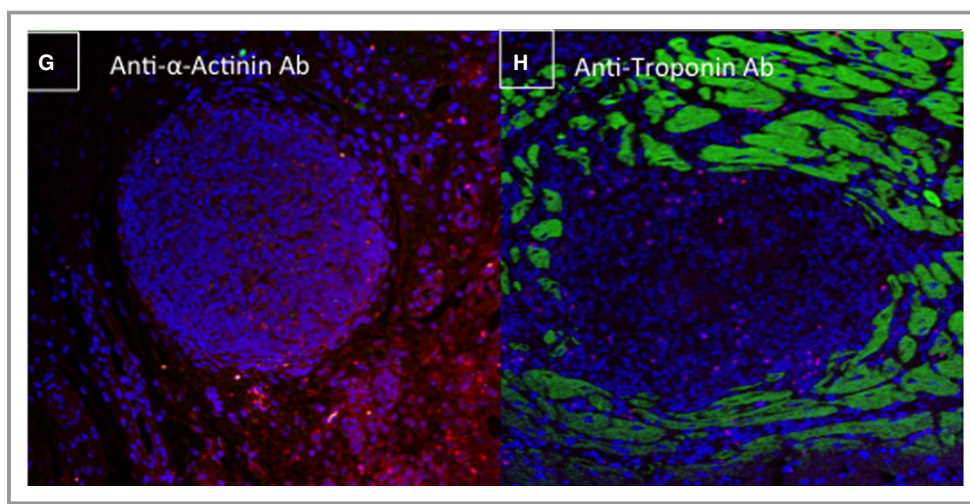
Figure 11. Continued

engrafted hAMSC clusters, whereas the PIR viability increased significantly, yielding 3 main conclusions: (1) The live hAMSCs do not differentiate into a cardiac lineage, (2) the mechanism of any functional benefit derived from cell delivery is likely paracrine, and (3) the regional functional restoration is likely due to salvage of the injured cardiomyocytes. Notably, the degree of functional restoration in both early and late–hAMSC animals was similar, suggesting that populations of at-risk or injured cardiomyocytes may exist in the PIR of both subacute and chronic ischemic cardiomyopathy, such that cell-restorative therapy may benefit both states. Finally, MEMRI as a contrast agent has been well studied in human subjects, and prior concerns about toxicity have been overcome by use of calcium supplementation.[16,25,26] Consequently, clinical trials of MEMRI in cell therapy are feasible today, and plans for MEMRI clinical trials are under way.

This study has several limitations. First, it is not clear to what extent MEMRI alone can distinguish healthy from injured cells. Currently, the overlap region between MEMRI and DEMRI is delineated to identify the PIR, which contains the injured cells.[16,25,26] Although the MEMRI signal was detectable with a significantly higher contrast/noise ratio within the injured myocardium, more investigation is required to delineate the resolution with which MEMRI can assess PIR viability. Second, quantification of the MEMRI signal is not always a discrete region but rather can be more diffuse, particularly on serial imaging. T1 mapping of the MEMRI signal may elucidate these diffuse processes. Third, the degree of myocardial salvage, regeneration, or stem cell engraftment cannot always be distinguished clearly. Recently, a group used diffusion tensor tractography in a mouse model and found that transplanted bone marrow mononuclear cells largely failed to generate new myofiber tracts required for engraftment.[27] Similarly, in this study, no evidence of cardiac differentiation

was observed by immunostaining; however, a threshold value in the change in MEMRI signal to differentiate salvage versus regeneration may be possible in future studies by correlating with the histological or other measures of cardiac phenotype of engrafted stem cells. Finally, MEMRI is equally feasible at 1.5-T field strength and may require direct comparison to 3 T.

In summary, this study demonstrates that stem cell–mediated functional restoration is associated with a sustained improvement in PIR viability and correlates closely with stem cell engraftment. MEMRI enables direct longitudinal assessment of PIR viability and represents a novel and robust method of imaging the therapeutic efficacy of transplanted stem cells in vivo.

Acknowledgments

Sources of Funding

Disclosures

Harnish is an employee of Eagle Vision Pharmaceutical Corporation. Wong Po Foo is an employee of Biocardia Inc.

References

1. Lloyd-Jones D, Adams R, Carnethon M, De Simone G, Ferguson TB, Flegal K, Ford E, Furie K, Go A, Greenlund K, Haase N, Hailpern S, Ho M, Howard V, Kissela B, Kittner S, Lackland D, Lisabeth L, Marelli A, McDermott M, Meigs J, Mozaffarian D, Nichol G, O'Donnell C, Roger V, Rosamond W, Sacco R, Sorlie P, Stafford R, Steinberger J, Thom T, Wasserthiel-Smoller S, Wong N, Wylie-Rosett J, Hong Y. Heart disease and stroke statistics—2009 update: a report from the American Heart Association Statistics Committee and Stroke Statistics Subcommittee. *Circulation*. 2009;119:480–486.

2. Heidary S, Patel H, Chung J, Yokota H, Gupta SN, Bennett MV, Katikireddy C, Nguyen P, Pauly JM, Terashima M, McConnell MV, Yang PC. Quantitative tissue characterization of infarct core and border zone in patients with ischemic cardiomyopathy by magnetic resonance is associated with future cardiovascular events. *J Am Coll Cardiol*. 2010;55:2762–2768.

3. Tsukiji M, Nguyen P, Narayan G, Hellinger J, Chan F, Herfkens R, Pauly JM, McConnell MV, Yang PC. Peri-infarct ischemia determined by cardiovascular magnetic resonance evaluation of myocardial viability and stress perfusion predicts future cardiovascular events in patients with severe ischemic cardiomyopathy. *J Cardiovasc Magn Reson*. 2006;8:773–779.

4. Jaussaud J, Biais M, Calderon J, Chevaleyre J, Duchez P, Ivanovic Z, Couffinhal T, Barandon L. Hypoxia-preconditioned mesenchymal stromal cells improve cardiac function in a swine model of chronic myocardial ischaemia. *Eur J Cardiothorac Surg*. 2012;43:1050–1057.

5. Kawamura M, Miyagawa S, Miki K, Saito A, Fukushima S, Higuchi T, Kawamura T, Kuratani T, Daimon T, Shimizu T, Okano T, Sawa Y. Feasibility, safety, and therapeutic efficacy of human induced pluripotent stem cell-derived cardiomyocyte sheets in a porcine ischemic cardiomyopathy model. *Circulation*. 2012;126:S29–S37.

6. Wright EJ, Farrell KA, Malik N, Kassem M, Lewis AL, Wallrapp C, Holt CM. Encapsulated glucagon-like peptide-1-producing mesenchymal stem cells have a beneficial effect on failing pig hearts. *Stem Cells Transl Med*. 2012;1:759–769.

7. Hung TC, Suzuki Y, Urashima T, Caffarelli A, Hoyt G, Sheikh AY, Yeung AC, Weissman I, Robbins RC, Bulte JW, Yang PC. Multimodality evaluation of the viability of stem cells delivered into different zones of myocardial infarction. *Circ Cardiovasc Imaging*. 2008;1:6–13.

8. Kaneda H, Ikeno F, Inagaki K, Mochly-Rosen D. Preserved coronary endothelial function by inhibition of delta protein kinase C in a porcine acute myocardial infarction model. *Int J Cardiol*. 2009;133:256–259.

9. Sun N, Lee A, Wu JC. Long term non-invasive imaging of embryonic stem cells using reporter genes. *Nat Protoc*. 2009;4:1192–1201.

10. Suzuki Y, Zhang S, Kundu P, Yeung AC, Robbins RC, Yang PC. In vitro comparison of the biological effects of three transfection methods for magnetically labeling mouse embryonic stem cells with ferumoxides. *Magn Reson Med*. 2007;57:1173–1179.

11. Yamada M, Gurney PT, Chung J, Kundu P, Drukker M, Smith AK, Weissman IL, Nishimura D, Robbins RC, Yang PC. Manganese-guided cellular MRI of human embryonic stem cell and human bone marrow stromal cell viability. *Magn Reson Med*. 2009;62:1047–1054.

12. Ge X, Wang IN, Toma I, Sebastiano V, Liu J, Butte MJ, Reijo Pera RA, Yang PC. Human amniotic mesenchymal stem cell-derived induced pluripotent stem cells may generate a universal source of cardiac cells. *Stem Cells Dev*. 2012;21:2798–2808.

13. Kim J, Lee Y, Kim H, Hwang KJ, Kwon HC, Kim SK, Cho DJ, Kang SG, You J. Human amniotic fluid-derived stem cells have characteristics of multipotent stem cells. *Cell Prolif*. 2007;40:75–90.

14. Parolini O, Alviano F, Bagnara GP, Bilic G, Buhring HJ, Evangelista M, Hennerbichler S, Liu B, Magatti M, Mao N, Miki T, Marongiu F, Nakajima H, Nikaido T, Portmann-Lanz CB, Sankar V, Soncini M, Stadler G, Surbek D, Takahashi TA, Redl H, Sakuragawa N, Wolbank S, Zeisberger S, Zisch A, Strom SC. Concise review: isolation and characterization of cells from human term placenta: outcome of the first international Workshop on Placenta Derived Stem Cells. *Stem Cells*. 2008;26:300–311.

15. Williams AR, Hatzistergos KE, Addicott B, McCall F, Carvalho D, Suncion V, Morales AR, Da Silva J, Sussman MA, Heldman AW, Hare JM. Enhanced effect of combining human cardiac stem cells and bone marrow mesenchymal stem cells to reduce infarct size and to restore cardiac function after myocardial infarction. *Circulation*. 2013;127:213–223.

16. Dash R, Chung J, Ikeno F, Hahn-Windgassen A, Matsuura Y, Bennett MV, Lyons JK, Teramoto T, Robbins RC, McConnell MV, Yeung AC, Brinton TJ, Harnish PP, Yang PC. Dual manganese-enhanced and delayed gadolinium-enhanced MRI detects myocardial border zone injury in a pig ischemia-reperfusion model. *Circ Cardiovasc Imaging*. 2011;4:574–582.

17. Suzuki Y, Lyons JK, Yeung AC, Ikeno F. The porcine restenosis model using thermal balloon injury: comparison with the model by coronary stenting. *J Invasive Cardiol*. 2008;20:142–146.

18. de la Fuente LM, Stertzer SH, Argentieri J, Penaloza E, Koziner B, Rouy D, Altman PA. Transendocardial autologous bone marrow in myocardial infarction induced heart failure, two-year follow-up in an open-label phase I safety study (the TABMMI study). *EuroIntervention*. 2011;7:805–812.

19. Kumar A, Haralampus CA, Hughes M, Rouy D, Cresswell N, Braun R, Turner D, Amrani D, Motlagh D, Schaer GL. Assessment of safety, accuracy, and human CD34+ cell retention after intramyocardial injections with a helical needle catheter in a porcine model. *Catheter Cardiovasc Interv*. 2013;81:970–977.

20. Trachtenberg B, Velazquez DL, Williams AR, McNiece I, Fishman J, Nguyen K, Rouy D, Altman P, Schwarz R, Mendizabal A, Oskouei B, Byrnes J, Soto V, Tracy M, Zambrano JP, Heldman AW, Hare JM. Rationale and design of the transendocardial injection of autologous human cells (bone marrow or mesenchymal) in chronic ischemic left ventricular dysfunction and heart failure secondary to myocardial infarction (TAC-HFT) trial: a randomized, double-blind, placebo-controlled study of safety and efficacy. *Am Heart J*. 2011;161:487–493.

21. Williams AR, Trachtenberg B, Velazquez DL, McNiece I, Altman P, Rouy D, Mendizabal AM, Pattany PM, Lopera GA, Fishman J, Zambrano JP, Heldman AW, Hare JM. Intramyocardial stem cell injection in patients with ischemic cardiomyopathy: functional recovery and reverse remodeling. *Circ Res*. 2011;108:792–796.

22. Li Z, Suzuki Y, Huang M, Cao F, Xie X, Connolly AJ, Yang PC, Wu JC. Comparison of reporter gene and iron particle labeling for tracking fate of human embryonic stem cells and differentiated endothelial cells in living subjects. *Stem Cells*. 2008;26:864–873.

23. Hendry SL II, van der Bogt KE, Sheikh AY, Arai T, Dylla SJ, Drukker M, McConnell MV, Kutschka I, Hoyt G, Cao F, Weissman IL, Connolly AJ, Pelletier MP, Wu JC, Robbins RC, Yang PC. Multimodal evaluation of in vivo magnetic resonance imaging of myocardial restoration by mouse embryonic stem cells. *J Thorac Cardiovasc Surg*. 2008;136:1028–1037.e1.

24. Vrtovec B, Poglajen G, Lezaic L, Sever M, Domanovic D, Cernelc P, Socan A, Schrepfer S, Torre-Amione G, Haddad F, Wu JC. Effects of intracoronary CD34+ stem cell transplantation in nonischemic dilated cardiomyopathy patients: 5-year follow-up. *Circ Res*. 2013;112:165–173.

25. Storey P, Chen Q, Li W, Seoane PR, Harnish PP, Fogelson L, Harris KR, Prasad PV. Magnetic resonance imaging of myocardial infarction using a manganese-based contrast agent (EVP 1001-1): preliminary results in a dog model. *J Magn Reson Imaging*. 2006;23:228–234.

26. Storey P, Danias PG, Post M, Li W, Seoane PR, Harnish PP, Edelman RR, Prasad PV. Preliminary evaluation of EVP 1001-1: a new cardiac-specific magnetic resonance contrast agent with kinetics suitable for steady-state imaging of the ischemic heart. *Invest Radiol*. 2003;38:642–652.

27. Sosnovik DE, Mekkaoui C, Huang S, Chen HH, Dai G, Stoeck CT, Ngoy S, Guan J, Wang R, Kostis WJ, Jackowski MP, Wedeen VJ, Kozerke S, Liao R. Microstructural impact of ischemia and bone marrow-derived cell therapy revealed with diffusion tensor magnetic resonance imaging tractography of the heart in vivo. *Circulation*. 2014;129:1731–1741.